Formation of long-lived resonances in hexagonal cavities by strong coupling of superscar modes

Qinghai Song,[1,2,*] Li Ge,[3] Jan Wiersig,[4] and Hui Cao[5]

[1]*Department of Electronic and Information Engineering, Shenzhen Graduate School, Harbin Institute of Technology, Shenzhen 518055, China*
[2]*National Key Laboratory of Tunable Laser Technology, Institute of Opto-Electronics, Harbin Institute for Technology, Harbin 150080, China*
[3]*Department of Electrical Engineering, Princeton University, Princeton, New Jersey 08544, USA*
[4]*Institut für Theoretische Physik, Universität Magdeburg, Postfach 4120, D-39016 Magdeburg, Germany*
[5]*Department of Applied Physics, Yale University, New Haven, Connecticut 06520-8482, USA*

(Received 16 June 2013; published 19 August 2013)

The recent progresses in single crystalline wide bandgap hexagonal disk have stimulated intense research attention on pursuing ultraviolet (UV) laser diodes with low thresholds. While whispering-gallery modes based UV lasers have been successfully obtained in GaN, ZnO nanorods, and nanopillars, the reported thresholds are still very high, due to the low-quality (Q) factors of the hexagonal resonances. Here we demonstrate resonances whose Q factors can be more than two orders of magnitude higher than the hexagonal modes, promising the reduction of the energy consumption. The key to our finding is the avoided resonance crossing between superscar states along two sets of nearly degenerated triangle orbits, which leads to the formation of hexagram modes. The mode couplings suppress the field distributions at the corners and the deviations from triangle orbits simultaneously and therefore enhance the Q factors significantly.

DOI: 10.1103/PhysRevA.88.023834 PACS number(s): 42.55.Sa, 42.55.Px, 81.07.Bc, 78.40.−q

I. INTRODUCTION

ZnO- or nitride-based UV laser diodes have been widely studied in past decade due to their applications ranging from chemical analysis, medical devices, bio-agent detection, and material processing to opto-electronics [1–3]. Compared with the bulky UV lasers, laser diodes have significant advantages, e.g., low cost, high efficiency, and compact size. A number of UV laser diodes have been demonstrated to work at short wavelengths or high quantum efficiency [4]. However, the thresholds of such UV lasers are usually very high. This is because that the severe challenge in mirror fabrication [5] gives very poor light confinements in the UV region [1–4]. In order to improve the light confinement, semiconductor microdisks [6–8], which can trap light by total internal reflection, have been employed to replace the conventional Fabry-Perot structures. Unfortunately, early approaches still suffered significant Q spoiling due to the surface roughness generated in the conventional top-down fabrication process [9,10].

Recently the bottom-up synthesized structures have attracted considerable research attention [11–21]. Compared with the top-down fabrication process, the bottom-up synthesis has inherent advantages such as single crystallinity, smooth surface faceting, and material homogeneity, which can effectively reduce the in-plane scattering loss. Meanwhile, the synthesis is usually independent of the choice of substrate and thus has the possibility to achieve better light confinement in vertical direction by selecting low refractive index substrate. Due to the improvements in light trapping, several groups have successfully demonstrated laser emissions from such synthesized structures [11–21]. However, the reported Q factors are only ∼1000, which is far below the initial expectations. This is mainly caused by the orbits of light confinements [22,23]. In general, the synthesized functional devices are typically wurtzite-type micro- and nanocrystals, which have hexagonal in-plane cross sections. The previous reported WG modes in hexagonal cavity are the resonances along the hexagonal orbit families. While the incident angles of hexagonal orbit families are far above the critical angle, these resonances usually have large field distributions around the sharp corners and thus experience the primary decay channels of polygonal microcavity, the boundary wave leakage, and the pesudointegrable leakage [23]. Therefore, finding a new type of resonances that are confined away from the corners will be highly desirable for pursuing the UV laser diodes with very low energy consumption.

II. RESULTS AND DISCUSSION

A. Periodic orbits families in hexagon-shaped microcavity

The typical microdisks are quasi-two-dimensional objects whose thicknesses are of the order of the wavelengths but with much larger in-plane dimensions. Thus a hexagonal microdisk can be treated as a two-dimensional hexagon-shaped cavity by applying an effective index of refraction n. We assume $n = 2.35$ (GaN or ZnO in UV region) for transverse electric (TE, E is in plane) polarization and ignore the material dispersion. In the hexagon-shaped microcavity, three different resonances with incident angle above the critical angle can be envisioned. The light can be confined along the hexagonal orbit families [Fig. 1(a)] with the equal incident angles of 60° and equal orbit lengths. The resonances along them have been first observed in Ref. [11] and then well explained by Refs. [22] and [23]. In addition, the light can also be trapped along the triangle orbits with incident angles of 30°. Due to the odd number of bouncing sides, the inscribed equilateral triangle orbit is isolated. The shortest periodic orbit family that can support the resonances with the low loss is twice longer [24].

Although the incident angles of triangle orbits are smaller than the hexagonal orbits, their abilities in trapping light can be even better. In general, the periodic orbits in polygon cavity form continuous families which can be unfolded to straight rectangle channels. The widths of the channels are

*qinghai.song@hitsz.edu.cn

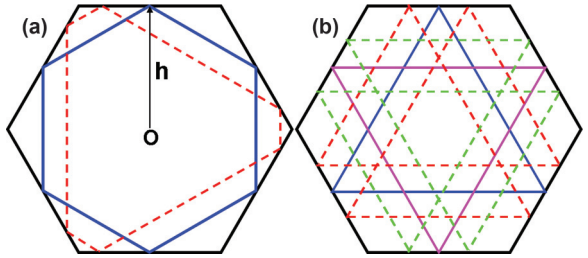

FIG. 1. (Color online) The periodic hexagonal orbit family (a) and periodic triangle orbit family (b) in hexagon-shaped microcavity. The solid line in (b) is the isolated triangle orbits. All the dashed and solid triangle orbits consist of $\bigtriangledown$ and $\bigtriangleup$ triangle orbit families and form the hexagram.

determined by the positions of the closest singular corners [24–26]. Taking into account all phase changes, the superscars formed along the orbit families can be considered as modes confined inside the rectangles, which are recorded by the mode number (m, p) along the lengths and widths of the rectangles, respectively [24]. As the width of rectangle formed by triangle orbit family (Channel T) is much wider than the one formed by hexagonal orbit family (Channel H), it is easy to find that the field distributions of high Q modes ($p = 1$) in Channel T are closer to the center and farther away from the sides of a rectangle, which are defined by straight lines passing through the corners. Therefore, the superscars in Channel T experience less scattering loss at the corners and can give higher Q factors.

More interestingly, the hexagonal cavity can form two sets of triangle orbit families with the same orbit lengths and reversed directions (up triangle $\bigtriangleup$ and down triangle $\bigtriangledown$) simultaneously. In conventional microcavity, the orbits with the same lengths are typically degenerated. In hexagonal cavity, such degeneracy has been lifted by the diffraction at the corners. Thus the superscars modes along both orbits families can have the the same eigenfrequencies. Meanwhile, two sets of triangle orbit families ($\bigtriangleup$ and $\bigtriangledown$) spatially overlap in the hexagon-shaped microcavity [see Fig. 1(b)] and form the hexagram, indicating the possibility of mode coupling [28] to improve the light confinement.

B. Avoided resonances crossings in hexagon-shaped microcavity

As we know, the resonant modes and their frequencies in microcavities can play the roles of states and their energies. Then the coupling between two resonant modes is usually understood in terms of a 2×2 matrix [27–29]:

$$H = \begin{pmatrix} E_1 & W \\ V & E_2 \end{pmatrix}, \tag{1}$$

where E_j are the energies and $\sqrt{VW}$ is the coupling strength. The hybrid states formed by mode coupling can be obtained from the eigenvalues of a 2×2 matrix:

$$E_{\pm}(\Delta) = \frac{E_1 + E_2}{2} \pm \sqrt{\frac{(E_1 - E_2)^2}{4} + VW} \tag{2}$$

In the case that $E_1 = E_2$, Eq. (2) can be rewritten as $E\pm = E_1 \pm \sqrt{VW}$. For the most general case of external coupling with $W \neq V^*$, we can find that the strong coupling can be naturally matched [here $|\mathrm{Im}(\sqrt{VW})| < |\mathrm{Im}(E_1)|$ is automatically matched to keep the solution reasonable for cold cavity]. Figure 2 illustrates such mode coupling effects. Different from the conventional strong coupling, we can find that both real parts and imaginary parts of energies are repulsive. The most important feature in Fig. 2(b) is that one state has a considerable lifetime enhancement and the other state has lifetime reduction at the ARC. Such dramatic lifetime modification provides a new approach to further achieve the Q factors of optical modes in microcavities.

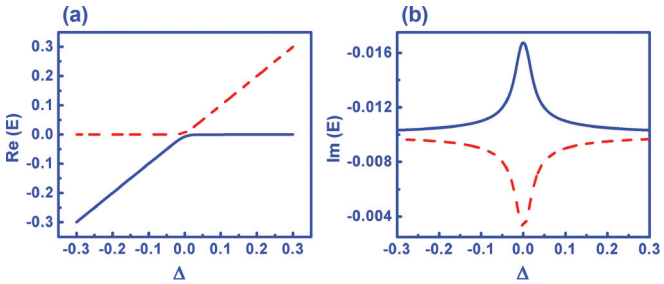

FIG. 2. (Color online) Mode coupling in the case of matrix (1) with $VW = i0.00008$, $E_1 = -i0.01$, $E_2 = \Delta - i0.01$. Real (a) and imaginary (b) part of the energy vs Δ.

C. Numerical simulation

We then numerically examine our analysis in the hexagon-shaped microcavity. All the resonances and their field patterns are calculated with a finite element method-based commercial software [29–31]. The open cavity is simulated by using a perfect matching layer to absorb the outgoing waves. As the open system does not have true bound states, the computed eigenvalues (kR) in optical microcavities are complex numbers. The real parts of kR give the positions of resonances, and the imaginary parts measure the losses due to the leakage from the cavity. Figure 3(a) shows the calculated resonances in a hexagon cavity, which is defined as [23]

$$\rho^s = \frac{R^s}{\left(\cos\phi - \frac{1}{\sqrt{3}}\sin\phi\right)^s + \left(\cos\phi + \frac{1}{\sqrt{3}}\sin\phi\right)^s + \left(\frac{2}{\sqrt{3}}\sin\phi\right)^s}. \tag{3}$$

Here we set $s = 200$ and $\phi = 0{:}\pi/3600{:}2\pi$ to make sure that the influences of rounding and deviation of cavity shape from Eq. (3) are negligible. From the constant mode spacings and similar field patterns, three types of resonances can be identified. The modes in series 3 are conventional WG-like resonances along the hexagonal orbit families, which give Q factors around 1000. One example is mode v in Fig. 3(a), whose field distribution is shown in Fig. 3(b). The modes in series 1 and series 2 are the superscars along the triangle orbit families. From their field patterns in Figs. 3(c) and 3(d) [modes i and vi in Fig. 3(a)], it is easy to know those modes correspond to the superscars with $p = 1$ and 2, respectively [24–26]. The Q factors of superscars with $p = 1$ are $> 10^4$, which are more than an order of magnitude higher than the modes along hexagonal orbit families. As the field distributions of modes along triangle orbits are away from the corners, their main leaky channels should be the pseudointegral leakage [23]. The solid line in Fig. 3(b) is the calculated Q factors formed by

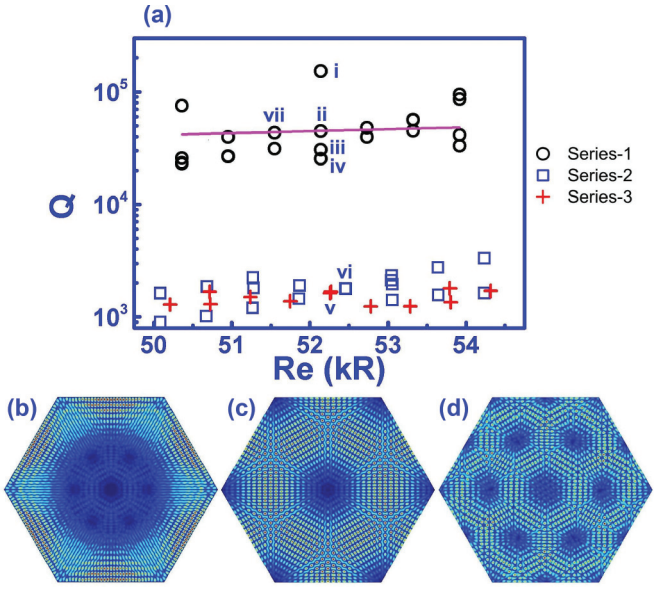

FIG. 3. (Color online) (a) The calculated resonances in a hexagon cavity inscribed to a circle with radius R. (b)–(d) The field patterns of resonances marked as v, i, and vi in Fig. 3(a), respectively. They are the examples of resonances in series 1, 2, and 3.

pesudointegrable leakage, which can be expressed as [23]

$$-\mathrm{Im}(\Omega) = \frac{1}{6n^2\mathrm{Re}(\Omega)}. \quad (4)$$

It qualitatively matches the Q factors of superscar with $p = 1$, giving evidence that the triangle orbit families can confine light better and generate higher Q factors. Actually, even the superscar with $p = 2$ [red crosses in Fig. 3(a)] can have similar Q factors as resonances in series 3.

The interesting phenomenon happens in the modes of series 1, where we can clearly see the periodicity of Q factors in Re(Ω). Some modes at $kR \approx 50.36$, 52.14, and 53.92 have Q factors above 10^5, which are about two orders of magnitude higher than the conventional hexagonal resonances. In Fig. 3(a) we can also find that the high-Q modes are always accompanied with the relative low-Q modes at the same kR [see modes i, ii, and modes iii, iv], indicating the possibility of an avoided resonance crossing (ARC).

To confirm the effect of mode coupling, we studied the resonances i–iv in Fig. 3(a) by shifting the top edge of the hexagon while keeping the two upper angles at 120°. We refer to the distance between the shifted edge to the original top side as δ and define $\varepsilon = 1 + \delta/(R \times \cos\pi/3)$. Interestingly, as the $\triangledown$ orbits are independent of the top side and the $\triangle$ orbits have bouncing points on it, changing ε can differ the resonant frequencies of superscars along $\triangle$ and $\triangledown$ orbit families. Figure 4 shows the calculated Re(Ω) and Im(Ω) as a function of ε. With the decreasing of ε from 1.001 to 0.999, the real parts of mode i (blue solid line) and mode iii (green dotted line) approach each other and repulse after $\varepsilon = 1$. Meanwhile, the imaginary parts of two modes show the anticrossing behavior simultaneously, giving the evidence of strong coupling with $E_1 = E_2$. Similar mode coupling has also been observed from modes ii and iv, which are shown as black dashed and red dash-dotted lines in Fig. 4.

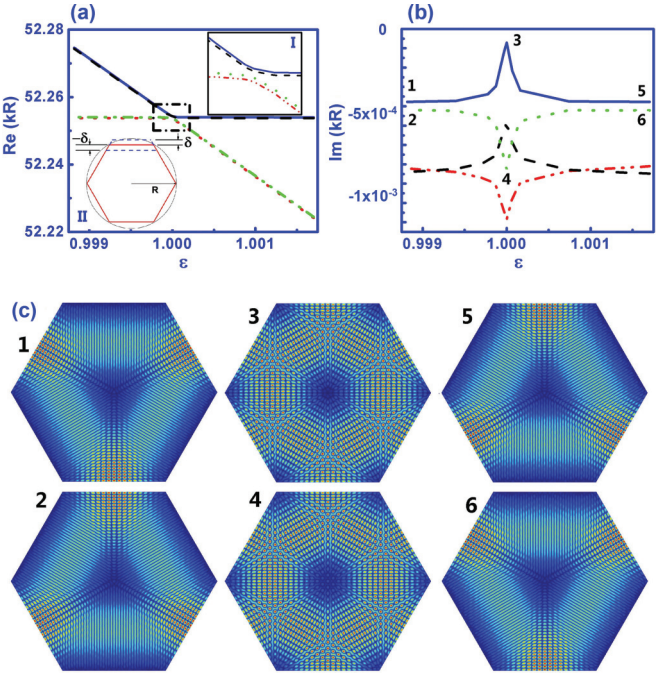

FIG. 4. (Color online) (a) and (b) are the real and imaginary parts of eigenvalues of modes i–iv in Fig. 3(a) as a function of ε. The resonances i–iv correspond to the solid line, dashed line, dotted line, and dash-dotted line, respectively. Both real and imaginary parts show clearly repulsive behaviors as Fig. 2. Here $\varepsilon = 1 + \delta/(R \times \cos\pi/3)$ and δ is defined as the separation distance between the shifted top edge (dashed) and the original one (solid) in the inset II in Fig. 4(a). (c) The field patterns of resonances marked as 1–6 in Fig. 4(b), and the exchange of identity can be observed.

Besides the repulsion in frequencies, strong coupling will also induce the exchange of identity [27–29,32]. In Fig. 4(c) mode 1 and mode 6 have roughly the same spatial profiles along $\triangledown$ orbits but belong to different frequency branches. The same holds true for mode 2 and mode 5. At ARC, mode 3 and mode 4 correspond to the hybrid modes of mode 1 and mode 2 (or mode 5 and mode 6). The mode coupling between two resonances with $E_1 = E_2$ usually happens in photonic molecules [33], where two microdisks couple with each other via the evanescent waves and each disk can support one resonance. The results in Fig. 4 are the first observation of such coupling in a single cavity, which does not require positioning the cavities precisely as the photonic molecules and thus have intrinsic advantages in applications. Moreover, as the spatial overlap happens in the field patterns directly, its influence on the Q factors are more significant than the photonic molecules, where the modes couple via the evanescent waves. Due to the different field distributions, the resonances along different orbit families can form either $\triangleleft\triangleright$ or $\triangleright\triangleleft$ in coupled hexagon-shaped microcavities. The maximum Q factors formed by the hexagonal photonic molecules is only ∼30 000, which is quite lower than mode i in Fig. 3.

D. Discussion

The physical mechanism behind the modification on Q factors can be understood as follows. The superscars along different orbit families will interfere each other as they have

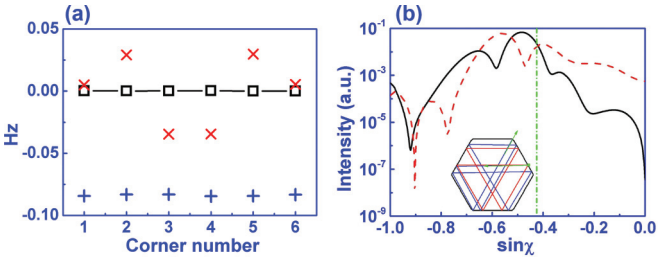

FIG. 5. (Color online) (a) Field distributions of hybrid mode i (open squares), mode iii (+), and mode vii (×) in Fig. 3(a) at the corners. The constructive interference doubles the field distribution (mode iii), and the destructive interference almost completely inhibits the intensity (mode i) of light at corners. (b) The calculated Husimi intensity of mode-i (solid line) and mode iii (dashed line) as a function of the angle of incidence. The vertical dotted line is the critical line, and the inset illustrates the deviation from the triangle orbit. In additional to the reduction of field distribution of mode i at the corner, the destructive interference can further suppress the intensity of light with small incident angle and thus gives Qfactors far above the others.

the same eigenfrequencies and spatial overlap. If the superscars have the same phases at the corners, constructive interference will happen and consequently enhance leakages at the corners. On the other hand, the reversed phases will induce destructive interference and reduce the field distributions at the corners. This can be confirmed by computing the field distribution at the corners. As shown in Fig. 5(a), the field distributions of mode i [relative high-Q mode in Fig. 3(a)] at the corner positions are destructively suppressed to almost 0, whereas the distributions of mode iii [relative low-Q mode in Fig. 3(a)] are an order of magnitude higher. Similar field distributions have also been observed in mode ii [relative high-Q mode in Fig. 3(a)] and mode iv [relative low-Q mode in Fig. 3(a)].

Different from the previous reports in Refs. [28,29], the main leakage here is the pesudointegrable leakage, which is the slight deviation from the original triangle orbit families [23]. Thus the relation between Q factors and field distributions at corners is not as straightforward as previously [28,29]. As schematically shown in the inset in Fig. 5(b), the deviated light will pretty much follow its original orbit. The angle of incidence is kept at $\sim 30^\circ$ before it drops to ~ 0 at the corners. Therefore, it is the intensity of light with small incident angle instead of the simple field distributions at the corners that dominates the decay channel.

In order to get such internal information, we have projected the internal mode structure onto the Poincaré surface of section (SOS) using a Husimi function [34,35]. The SOS can give ray content of the resonance in terms of a density of rays and their angle of incidence. Figure 5(b) shows the normalized Husimi intensity at one corner as a function of incident angle χ. The field distribution below critical angle of mode iii is orders of magnitude higher than mode i. We thus know that the destructive interference can suppress the deviation of mode i from triangle orbits besides the inhibition of field distribution at the corners. This is consistent with the dramatic increasing Q factor of mode i in Fig. 3(a). For the case of mode iii, a totally reversed process happens and thus gives a reduction in Q factor.

It is worth noting that all the superscar modes along different triangle orbit families will couple with one another if they have the same eigenvalues. Thus the simply constructive and destructive interference cannot well explain the dependence of Q factor on Re(Ω). To reveal the reason for the fluctuation of Q factor in series1, we have to further consider the quantum numbers (m) of superscar modes [25]. As shown in Fig. 3(a), we can see that all the dramatic changes in Q factors happen at the quantum numbers that are divisible by three. If the modes along different orbits have a 0 or π phase difference in one corner, the same difference can be transported to the other corners due to the integer quantum number along each side of the triangle orbit (phase changes caused by the transportation can be expressed as $\Phi = 2\pi \times \frac{m}{3}$, where m is divisible by three). Therefore, the same constructive or destructive interference will happen simultaneously at all corners and modify the Q factors significantly [see open squares and + in Fig. 5(a)]. On the other hand, if the quantum numbers are not divisible by three, the phase difference between modes along different orbits cannot be the same at all corners. Thus the completely destructive interference occurs only at a few corners [see the × in Fig. 5(a)], and its consequent influence on Q factors is much weaker in Fig. 3(a).

III. CONCLUSIONS

In summary, we have studied the formation of long-lived resonances in hexagon-shaped microcavities. We show that the triangle orbit families ($\triangle$ and $\triangledown$) can confine light away from the corners. Thus the resonances experience less boundary wave leakage and give a higher Q factor than the previous reported WG-like modes. More interestingly, we show that two resonances along the $\triangle$ and $\triangledown$ orbit families can couple with each other and further enhance the light localization by decreasing the pseudointegrable leakage with destructive interference. Our finding will shed light on the development of UV or deep-UV microdisk lasers and filters.

As the single crystalline microdisks are nearly perfect, the high-Q resonances formed by ARCs have the possibility to be observed in real systems [18]. It is therefore important to note the field of application of our numerical solutions. Besides the microdisk with wavelength-scale thickness [18] discussed above, our results can also be applied in nanorods and nanowires, where the TE and TM modes are exactly the solutions of two-dimensional Helmholtz equations [21–23]. Once the thickness is close to an in-plane size [20], the situation becomes more complicated. Our results can still be used to understand some phenomena qualitatively. However, the detailed information must be calculated with a full three-dimensional calculation to get the HE or EH resonances as in Ref. [16].

ACKNOWLEDGMENTS

This work is supported partly by the NSFC under Grant Nos. 11204055 and 61222507. The authors also would like to thank support by the open project of the State Key Laboratory on Integrated Optoelectronics under the Grants No. 2011KFB005 and No. 2011KFB009.

[1] M. H. Huang, S. Mao, H. Feick, H. Q. Yan, Y. Y. Wu, H. Kind, E. Weber, R. Russo, and P. D. Yang, Science **292**, 1897 (2001).
[2] Y. Taniyasu, M. Kasu, and T. Makimoto, Nature (London) **441**, 325 (2006).
[3] H. Yoshida, Y. Yamashita, M. Kuwabara, and H. Kan, Nat. Photon. **2**, 551 (2008).
[4] Y. Yamashita, M. Kuwabara, K. Torii, and H. Yoshida, Opt. Express **21**, 3133 (2013).
[5] H. Lohmeyer *et al*., Eur. Phys. J. B **48**, 291 (2005).
[6] S. L. Mccall *et al*., Appl. Phys. Lett. **60**, 289 (1993).
[7] C. P. Michael *et al*., Appl. Phys. Lett. **90**, 051108 (2007).
[8] Q. H. Song, L. Ge, B. Redding, and H. Cao, Phys. Rev. Lett. **108**, 243902 (2012).
[9] G. D. Chern *et al*., Appl. Phys. Lett. **83**, 1710 (2003).
[10] A. C. Tamboli *et al*., Nat. Photon. **1**, 61 (2007).
[11] U. Vietze, O. Krauß, F. Laeri, G. Ihlein, F. Schüth, B. Limburg, and M. Abraham, Phys. Rev. Lett. **81**, 4628 (1998).
[12] K. Hiramatsu *et al*., J. Cryst. Growth **221**, 316 (2000).
[13] C. Kim, Y.-J. Kim, E.-S. Jang, G.-C. Yi, and H. H. Kim, Appl. Phys. Lett. **88**, 093104 (2006).
[14] H. X. Dong *et al*., Appl. Phys. Lett. **94**, 173115 (2009).
[15] A. R. Smith, R. M. Feenstra, D. W. Greve, J. Neugebauer, and J. E. Northrup, Phys. Rev. Lett. **79**, 3934 (1997).
[16] D. J. Gargas, M. C. Moore, A. Ni, S.-W. Chang, Z. Y. Zhang, S.-L. Chuang, and P. D. Yang, ACS Nano **4**, 3270 (2010).
[17] G. P. Zhu *et al*., Appl. Phys. Lett. **94**, 051106 (2009).
[18] T. Kouno, K. Kishino, and M. Sakai, IEEE J. Quantum Electron. **47**, 1565 (2011).
[19] T. Nobis, E. M. Kaidashev, A. Rahm, M. Lorenz, and M. Grundmann, Phys. Rev. Lett. **93**, 103903 (2004).
[20] C. Tessarek, G. Sarau, M. Kiometzis, and S. Christiansen, Opt. Express **21**, 2733 (2013).
[21] M. Grundmann and C. P. Dietrich, Phys. Status Solidi B **249**, 871 (2012).
[22] I. Braun *et al*., Appl. Phys. B **70**, 335 (2000).
[23] J. Wiersig, Phys. Rev. A **67**, 023807 (2003).
[24] M. Lebental, N. Djellali, C. Arnaud, J.-S. Lauret, J. Zyss, R. Dubertrand, C. Schmit, and E. Bogomolny, Phys. Rev. A **76**, 023830 (2007).
[25] E. Bogomolny and C. Schmit, Phys. Rev. Lett. **92**, 244102 (2004).
[26] E. Bogomolny, B. Dietz, T. Friedrich, M. Miski-Oglu, A. Richter, F. Schäfer, and C. Schmit, Phys. Rev. Lett. **97**, 254102 (2006).
[27] W. D. Heiss, Phys. Rev. E **61**, 929 (2000).
[28] J. Wiersig, Phys. Rev. Lett. **97**, 253901 (2006).
[29] Q. H. Song and H. Cao, Phys. Rev. Lett. **105**, 053902 (2010).
[30] Commercial program Comsol Multiphysics 3.5a.
[31] M. I. Cheem and A. G. Kirk, Opt. Express **21**, 8724 (2013).
[32] S.-B. Lee, J. Yang, S. Moon, S.-Y. Lee, J.-B. Shim, S. W. Kim, J.-H. Lee, and K. An, Phys. Rev. Lett. **103**, 134101 (2009).
[33] M. Benyoucef, J.-B. Shim, J. Wiersig, and O. G. Schmidt, Opt. Lett. **36**, 1317 (2011).
[34] M. Hentschel, H. Schomerus, and R. Schubert, Europhys. Lett. **62**, 636 (2003).
[35] H. E. Türeci, H. G. L. Schwefel, P. Jacquod, and A. D. Stone, Prog. Opt. **47**, 75 (2005).